Chapter 6

Mechanical and Fracture Properties of Carbon Nanotubes

Keiichi Shirasu, Go Yamamoto, Daniel Nelias and Toshiyuki Hashida

Additional information is available at the end of the chapter

http://dx.doi.org/10.5772/intechopen.70578

Abstract

Carbon nanotubes (CNTs) have attracted much interest because of their superior electrical, thermal, and mechanical properties. These unique properties of CNTs have come to the attention of many scientists and engineers worldwide, eager to incorporate these novel materials into composites and electronic devices. However, before the utilization of these materials becomes mainstream, it is necessary to develop protocols for tailoring the material properties, so that composites and devices can be engineered to given specifications. In this chapter, we review our recent studies, in which we investigate the nominal tensile strength and strength distribution of multi-walled CNTs (MWCNTs) synthesized by the catalytic chemical vapor deposition (CVD) method, followed by a series of high-temperature annealing steps that culminate with annealing at 2900°C. The structural-mechanical relationships of such MWCNTs are investigated through tensile-loading experiments with individual MWCNTs, Weibull-Poisson statistics, transmission electron microscope (TEM) observation, and Raman spectroscopy analysis.

Keywords: carbon nanotubes, tensile strength, Weibull-Poisson statistics, structural defects, heat treatment

1. Introduction

Carbon nanotubes (CNTs) have attracted much interest because of their potential application as next-generation electronic and structural materials. In particular, their superior electrical, thermal, and mechanical properties, including high electrical and thermal conductivity [1, 2], negative thermal expansion coefficient [3–10], and high mechanical strength, exceeding 100 GPa [11, 12], make them a candidate material for nano- and microscale composites,

sensors, actuators, and other electronic devices. Additionally, continuous multi-walled CNT (MWCNT) yarns and sheets, which are prepared by directly drawing MWCNTs from spinnable MWCNT arrays, have been developed [13, 14], and new processing methods utilizing MWCNT yarns and sheets have emerged as means of producing preforms and composites with higher MWCNT volume fractions [15–25]. The most recent reviews on these topics were reported by Di et al. [26] and Goh et al. [27].

The Young's modulus and strength of CNTs are well known to depend critically on the structure (e.g., geometry, crystallinity, and defect type and density), which in turn depends on the manufacturing route and subsequent treatment [28–31]. Quantum mechanics calculations [32–36] predict that defect-free single-walled CNTs possess Young's modulus values of ~1 TPa, tensile strengths >100 GPa, and failure strains of ~15–30%, depending on the chirality. However, experimental measurements [29, 37–41], which have all involved MWCNTs, have reported markedly lower values for fracture strengths and failure strains. For example, Ding et al. [40] showed that unpurified arc discharge-grown MWCNTs yielded a mean modulus value of 955 GPa, in good agreement with theory, but mean fracture strengths and failure strains that were only 24 GPa and 2.6%, respectively. Calculations [35] have suggested that defects introduced by oxidative pitting during nanotube purification can markedly reduce fracture strength. Therefore, for the development of basic design concepts for the use of CNTs in nanocomposites that require high strength, experimental evaluation of the mechanical properties of CNTs is crucial.

Several techniques have been developed for exploring the mechanical properties of individual CNTs. One method for measuring the Young's modulus of a CNT is to fabricate a nanotube beam that is clamped at each end to a ceramic membrane (or otherwise supported) and to measure its vertical deflection versus the force applied at a point midway along its length [28]. The atomic force microscope (AFM) is a natural and convenient means for studying the Young's modulus of CNTs, because it allows measurement of the deflection of a sample as a function of applied force when used in contact mode [28, 30, 42–46]. Salvetat et al. [28] deposited a droplet of a MWCNT suspension on a well-polished alumina ultrafiltration membrane and evaluated the Young's modulus using the abovementioned method. They found that MWCNTs grown by catalytic chemical vapor deposition (CVD) have Young's moduli in the range of 12–50 GPa (mean: 27 GPa). These values are considerably lower than the moduli of arc discharge-grown MWCNTs (600–1100 GPa). Recently, Elumeeva et al. [30] investigated the Young's modulus of four types of MWCNTs synthesized by the CVD method followed by a series of high-temperature annealing steps at 2200, 2600, and 2800°C using a method similar to that of Salvetat et al.'s study [28]. The experimental results showed that the Young's modulus increased for the annealed MWCNTs with respect to the as-grown ones. Poncharal et al. presented a vibrating reed technique for testing the bending modulus of MWCNTs [47]. The elastic bending modulus as a function of diameter was found to decrease sharply (from approximately 1 TPa to 100 GPa) with increasing diameter (from 8 to 40 nm), which was attributed to the crossover from a uniform elastic mode to an elastic mode

that involves wavelike distortions in the nanotube. Gaillard et al. [48] also used a similar experimental setup, but their technique is relatively simpler: the resonance frequency of an electrostatically driven MWCNT is determined using a dark-field optical microscope. They found that there was a correlation between the defect density and the bending modulus, which suggests that the bending modulus is relatively more sensitive to wall defects than the nanotube diameter. The other method for evaluation of the tensile strength and Young's modulus of CNTs is the tensile testing method [11, 12, 37–41, 49–51]. Yu et al. [37] measured the stress-strain response and strength at failure of individual arc discharge-grown MWCNTs (~30 μm long) using a manipulator tool operated inside a scanning electron microscope (SEM). They reported measured tensile strengths and Young's moduli of MWCNTs ranging from ~11 to ~63 GPa and from 270 to 950 GPa, respectively. Peng et al. [11] reported that defect-free individual MWCNTs were shown to possess a mechanical strength equivalent to the theoretical value (100 GPa) using a precise in situ transmission electron microscopy (TEM) method with a micro-electromechanical system (MEMS) material testing system. They also performed a study on the effect of electron irradiation parameters on the resulting MWCNT strength. They found that as the irradiation-induced defect density increased, the tensile strength decreased, with that of three nonirradiated samples and a sample irradiated at a higher dose being ~100 GPa on average and 35 GPa, respectively. Yamamoto et al. [29] performed a study of the effect of acid treatment on the tensile strength of CVD-grown MWCNTs (~9 μm long), using a piezo-actuated nanomanipulator. The acid treatment introduced deep nanoscale defects as well as negatively charged functional groups onto the surface of the MWCNTs. The defects in these acid-treated MWCNTs had a channel-like structure, as if a ring of material was cut away from the MWCNT around its circumference [29]. By comparing the SEM images of MWCNTs acquired before and after fracture, it was found that all the nanotubes tested fractured in the so-called *sword-in-sheath failure* mode; the fracture of the acid-treated MWCNTs mostly occurred at the nanodefects. Tensile-loading experiments revealed that the tensile strengths of pristine MWCNTs were in the range of 2–48 GPa (mean, 20 GPa). However, the acid-treated MWCNTs with nanoscale defects possessed a tensile strength of 1–18 GPa (mean, 6 GPa), which is approximately 70% lower than that of the pristine MWCNTs. These results indicated that the channel-like defects associated with the acid etching were typically the weakest points in the acid-treated MWCNT structure and that stress concentration was present at the defect region. In these studies, the tensile strength was calculated from either the fractured cross-sectional area (effective strength) or the cross-sectional area of the outermost layer of the MWCNT. Few research groups have examined the nominal (or *engineering*) strength and its Weibull distribution, which are required for investigations of crack bridging characteristics and mechanical properties of composites reinforced with MWCNTs (a detailed discussion is given in [52]). Yu et al. [37] calculated the nominal tensile strengths to be in the range of 1.4–2.9 GPa, which is much lower than the effective tensile strength (11–63 GPa).

Here, we review our recent studies in which the strength properties of individual MWCNTs synthesized by a CVD method, followed by a series of high-temperature annealing steps that culminate with annealing at 2900°C, are investigated by a manipulator tool operated inside

an SEM [52–54]. The relationship between the MWCNT structure and strength properties of MWCNTs with a significantly different nanostructure is investigated through tensile tests of individual MWCNTs, transmission electron microscope (TEM) observations, and Raman spectroscopy analysis.

2. Structural characterization of carbon nanotubes

MWCNT materials (acquired from Hodogaya Chemical, Japan) synthesized by a catalytic CVD process were thermally annealed in a graphite crucible using a resistance-heated graphite element furnace at 1200, 1800, 2200, and 2600°C under an argon atmosphere [53]. The temperature was raised at a heating rate of approximately 60°C/min to the predetermined temperature and held there for 1 h before cooling to ambient temperature. The average outer diameter, inner diameter, and length of the MWCNTs are approximately 70, 7 nm and 7.8 μm, respectively. **Figure 1** shows typical TEM images of the four types of MWCNTs. At an annealing temperature of 1200°C (**Figure 1a**), the sample consists of turbostratic elementary domains 2–3 graphene layers thick. Each elementary domain is tilted at an angle with respect to the nanotube axis, forming larger wrinkled layers. When the annealing temperature increased to 1800°C (**Figure 1b**), the turbostratic structure disappears, and instead undulated fringes are formed by hooking the adjacent elementary domains together, i.e., both the in-plane and c-axis crystallite sizes appear to increase in this temperature range. For the samples annealed at 2200°C (**Figure 1c**), even though the undulated structure seems to remain unchanged, the graphitic planes become aligned, and the crystallite sizes increase further. With thermal annealing at 2600°C (**Figure 1d**), the undulating structure disappears, and the MWCNTs consist of nested graphitic cylinders that are almost perfectly aligned with the nanotube axis. However, these MWCNTs are observed to possess structural defects such as abrupt structural changes from constant-diameter cylinders and unevenly spaced lattice fringes. Hereafter, these kinds of MWCNTs are referred to as H-MWCNTs.

Spinnable MWCNT arrays were obtained by a thermal CVD method using C_2H_2 and $FeCl_2$ as the base material and the catalyst, respectively. The procedure for the fabrication of the MWCNT arrays follows [55]. The average outer diameter and inner diameter were approximately 40 and 7 nm, respectively, and the length of the MWCNTs was ~700 μm. The MWCNTs were thermally annealed in a graphite crucible (Kurata Giken SCC-U-80/150) using a resistance-heated graphite element furnace at 2000°C in a vacuum, followed by heat treatment at 2400 and 2900°C under an argon atmosphere. **Figure 2** shows TEM images of some of the MWCNTs. The as-grown MWCNTs consist of slightly undulating graphitic cylinders with respect to the nanotube axis (**Figure 2a**). Additionally, these MWCNTs possess several types of structural defects, such as *kinks and bends*, *discontinuous flaws*, and *remnant catalysts* (**Figure 2c–f**). For the samples annealed at 2400°C, the degree of waviness of the nanotube walls seems to decrease. Following thermal annealing at 2900°C (**Figure 2b**), the undulated structure disappears, and the MWCNT consists of nested graphitic cylinders that are almost perfectly aligned with the nanotube axis. However, structural defects such as *discontinuous flaws* and *kinks and bends* are still observed for a subset of the samples. The structural defect densities for the MWCNTs prepared in this study are summarized in **Table 1**. The thermally

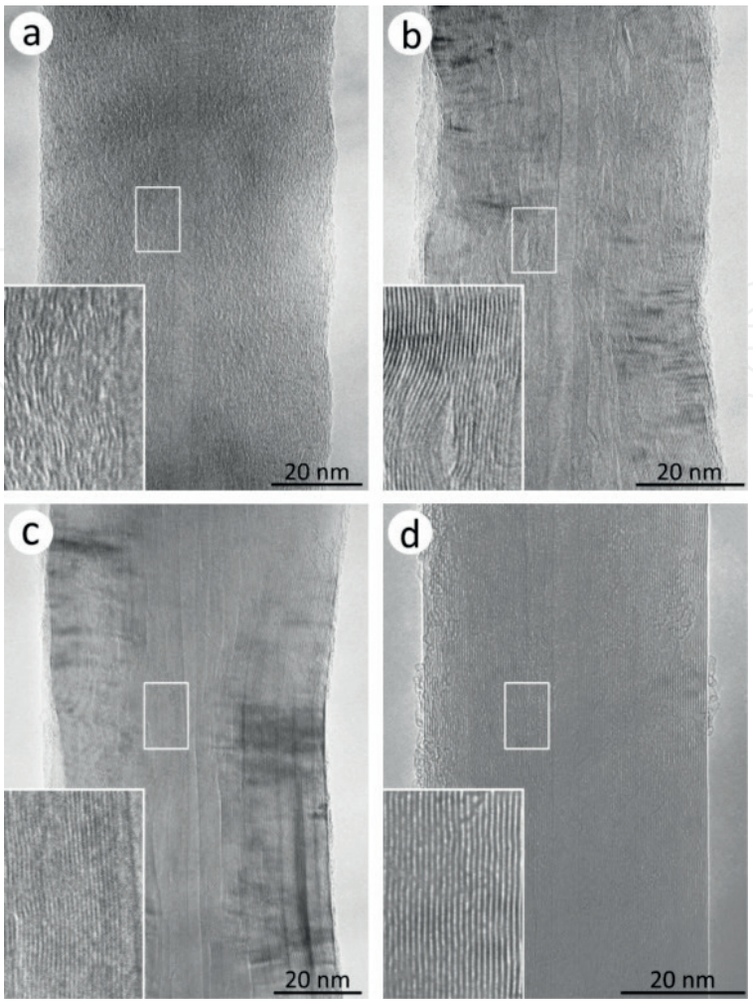

Figure 1. TEM images showing structural evolution of H-MWCNTs [53]. Annealing temperatures are (a) 1200°C, (b) 1800°C, (c) 2200°C, and (d) 2600°C.

annealed MWCNTs possessed a smaller amount of structural defects, characterized by *discontinuous flaws* and *kinks and bends* and no *remnant catalyst* compared with the as-grown MWCNTs. In this chapter, we call these nanotubes S-MWCNTs.

Next, we used Raman spectroscopy to evaluate whether any structural evolution occurs during thermal annealing. The Raman scattering spectrum of the MWCNTs shows a pair of bands around 1360 cm^{-1} (D-band) and 1590 cm^{-1} (G-band) [56]. Thus, the relative intensity ratio of the G-band to D-band peak, i.e., $R = I_G/I_D$, is known to depend on the number of defects in the nanotubes [57]. The Raman intensity ratios (R) of the H-MWCNTs and S-MWCNTs are shown in **Figure 3**. The Raman spectra of the MWCNTs showed a pair of bands near 1360 and 1590 cm^{-1}. The R values of the H-MWCNTs increased from 1.0 to 10.1 with increasing annealing temperature. For the S-MWCNTs, there is no clear difference in the R values between the as-grown MWCNTs and those annealed at 2000°C (R = 3.2 and 3.8), suggesting that both types of MWCNTs have the same degree of crystallinity. On the other hand, the R values increase with increasing annealing temperature over the temperature range 2000–2900°C

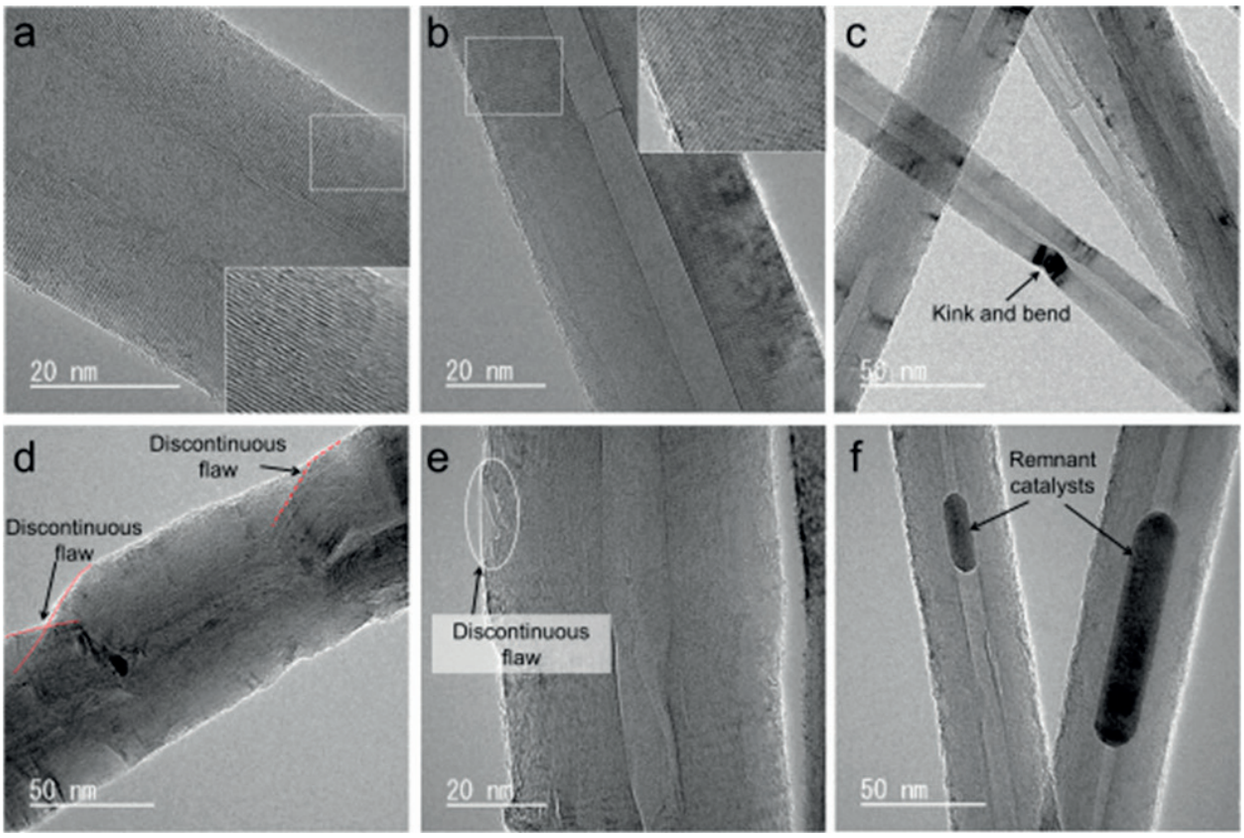

Figure 2. TEM images of the (a, c-f) as-grown S-MWCNTs and (b) MWCNTs thermally annealed at 2900 °C [52]. Arrows indicate the position of structural defects such as (c) *kinks and bends*, (d, e) *discontinuous flaws* (i.e., discontinuity in nanotube layers and *voids and holes*), and (f) *remnant catalyst*.

Annealing temperature (°C)	Kinks and bends (/μm)	Discontinuous flaws (/μm)	Remnant catalysts (/μm)
As-grown	1.9	6.4	1.2
2400	1.1	2.5	0
2900	1.6	1.7	0

Table 1. Structural defect densities for three types of S-MWCNTs [52].

(R = 23.3). This result suggests that defects in the structure of the MWCNTs were removed by annealing to produce a more stable graphite planar structure.

3. Tensile properties

3.1. Fracture behavior

Uniaxial tensile tests on individual MWCNTs were carried out with a manipulator inside the vacuum chamber of a SEM (JEOL JSM6510), as shown in **Figure 4**. Further details of the experimental procedure are described elsewhere [29]. In brief, AFM cantilevers served as

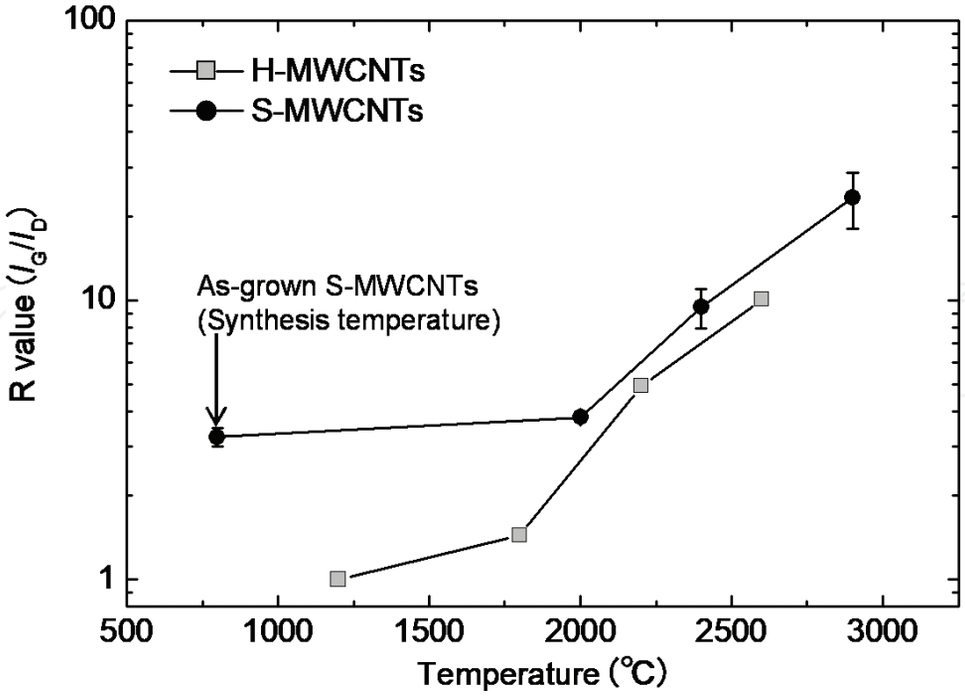

Figure 3. Raman intensity ratio as a function of MWCNT annealing temperature [52, 53].

force-sensing elements, and the force constants of each were obtained in situ prior to the tensile tests using the resonance method developed by Sader et al. [58]. An individual MWCNT was clamped onto the cantilever tip by local electron-beam-induced deposition (EBID) of a carbonaceous material [59]. The applied force can be calculated as follows (**Figure 1d**):

$$F = k(\Delta x - \Delta L) \tag{1}$$

where k is the force constant, Δx is the displacement of the cantilever, and ΔL is the nanotube elongation. The nanotube elongation was determined by counting the number of pixels in the acquired SEM images. The movement rate of the XY motion stage of the manipulator for the tensile tests was approximately 0.1 μm/s. After the MWCNT broke, both cantilevers with attached MWCNT fragments were transferred to a TEM sample stage and examined in the TEM to determine the outer diameters. We measured the full cross-sectional area, including the inner hole of each of the broken MWCNTs, using TEM and used the measured values to calculate the tensile strength.

The fracture morphology of MWCNTs is divided into two groups: the complete fracture of nanotube walls (*clean break* or *sword and sheath failure* mode) and *sword-in-sheath failure* mode, which depends on their crystallinity and existence of structural defects. Two series of SEM and TEM images for each of the two individual H-MWCNTs, captured before and after breaking, are shown in **Figure 5**. In the first series (**Figure 5A1–A5**), a H-MWCNT annealed at 1800°C with a gauge length of 13.1 μm was clamped onto the cantilever and tungsten wire tips by local EBID and then loaded in increments until failure. After breaking, the fragment of the same MWCNT attached to the cantilever tip had a length of 13.3 μm (**Figure 5A2** and **A4**). The other fragment of the same MWCNT attached to the tungsten wire had a length of at least 0.2 μm (**Figure 5A3**

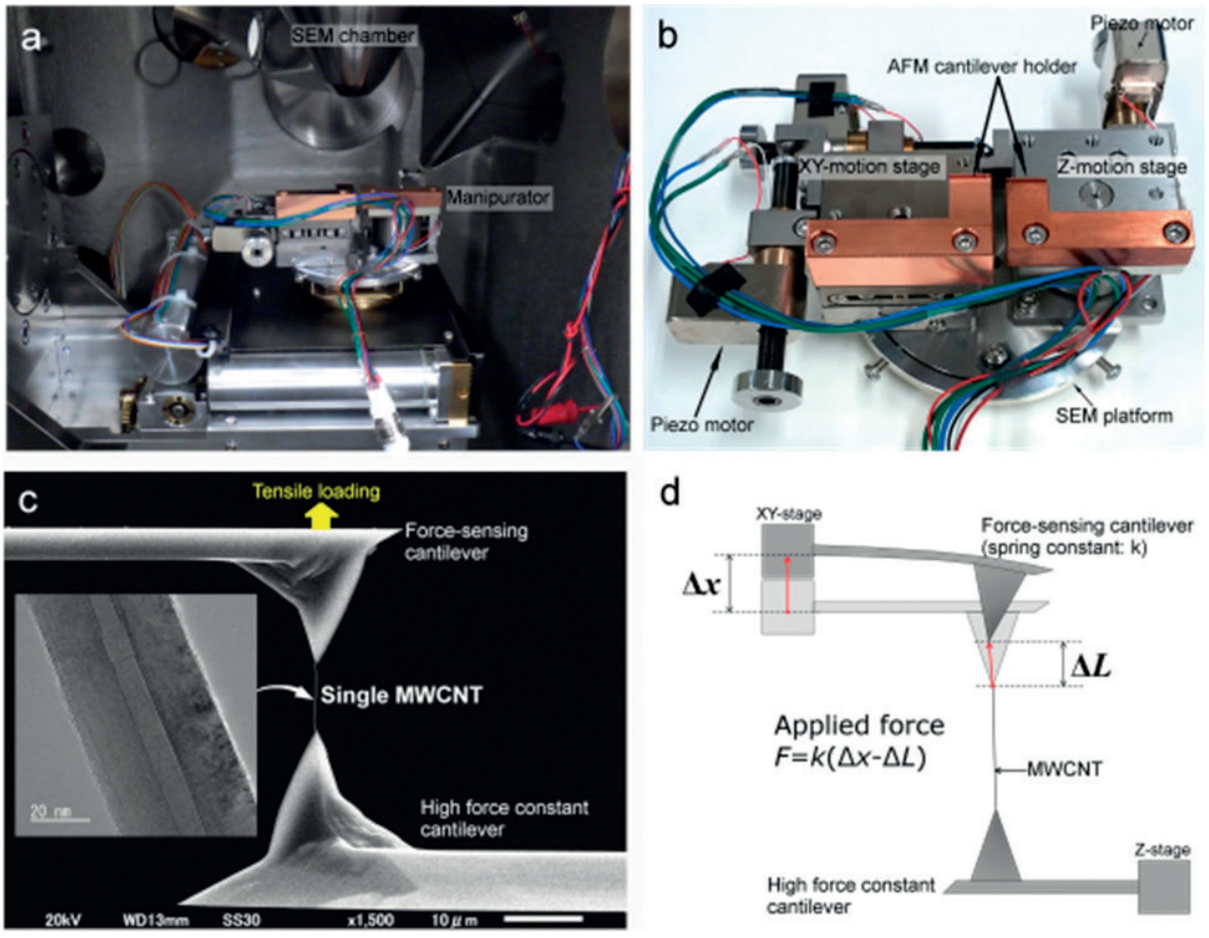

Figure 4. (a, b) Nanomanipulator system used for tensile tests on individual MWCNTs. (c) A SEM image of two AFM cantilever tips holding a MWCNT, which is attached at both ends to the AFM silicon tip surface by electron beam deposition of carbonaceous material. (d) Schematic description of cantilever displacement during the tensile test.

and **A5**), indicating that the MWCNT underwent failure in the so-called clean break manner (**Figure 6A1–A3**), as observed for CVD-grown MWCNTs under tensile loading [38]. Similar *clean break*-type failure was observed for H-MWCNTs annealed at 1200 and 2200°C. In contrast, the H-MWCNTs annealed at 2600°C broke in the outer walls, and the inner core was pulled away from the outer walls (**Figure 5B1–B3**), i.e., they underwent failure in a *sword-in-sheath failure* mode (**Figure 6B1–B3**), as observed for arc discharge-grown MWCNTs under tensile loading [11, 37]. An 11.1-μm-long section of this MWCNT was loaded and fractured in the middle of the gauge length. The resulting fragment attached to the cantilever tip had a length of at least 2.4 μm (**Figure 5B2**), whereas the other fragment on the tungsten wire had a length of at least 10.6 μm (**Figure 5B3**). Thus, the sum of the fragment lengths far exceeded the original section length. This apparent discrepancy can be explained as resulting from a *sword-in-sheath*-type failure.

Next, SEM and TEM images of an individual as-grown S-MWCNT linked between two opposing AFM cantilever tips before and after tensile loading are shown in **Figure 7**. An as-grown S-MWCNT having a gauge length of 3.2 μm was clamped onto the cantilevers and then loaded in increments until failure. After breaking, the fragment of the same MWCNT attached to the high-force constant cantilever tip had a length of 0.5 μm (**Figure 7b1**), while

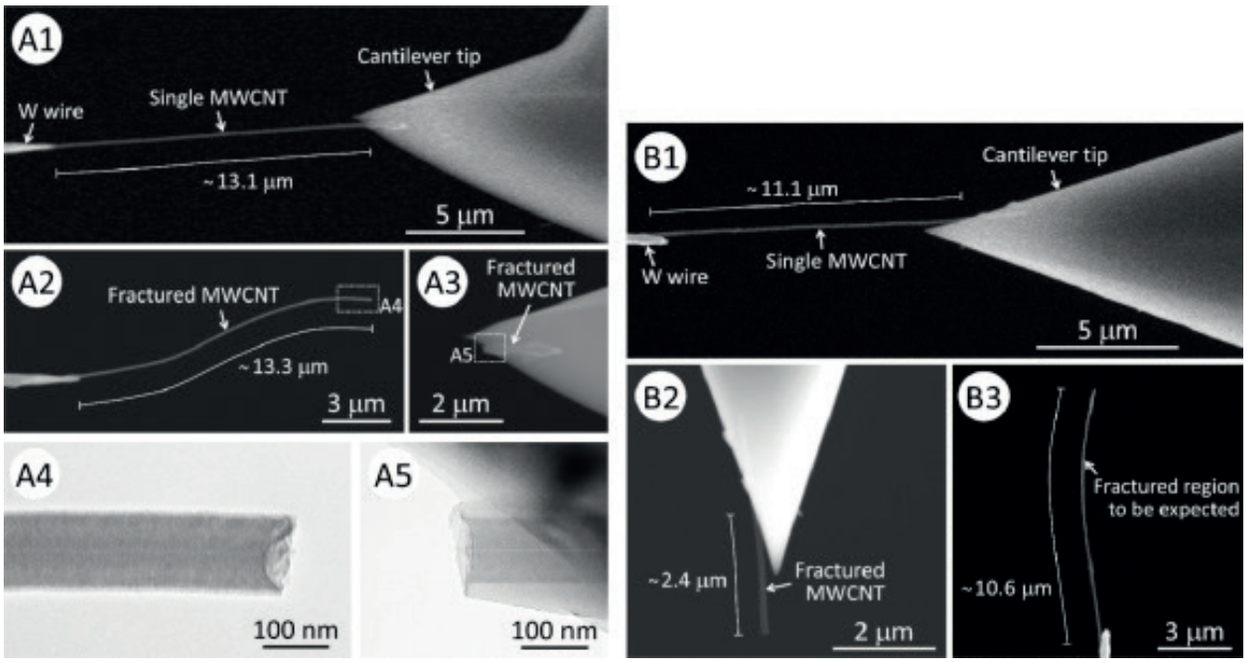

Figure 5. Two series of SEM and TEM images for each of two individual H-MWCNTs, captured before and after their breaking [53]. Annealing temperatures are (A1–A5) 1800°C and (B1–B3) 2600°C.

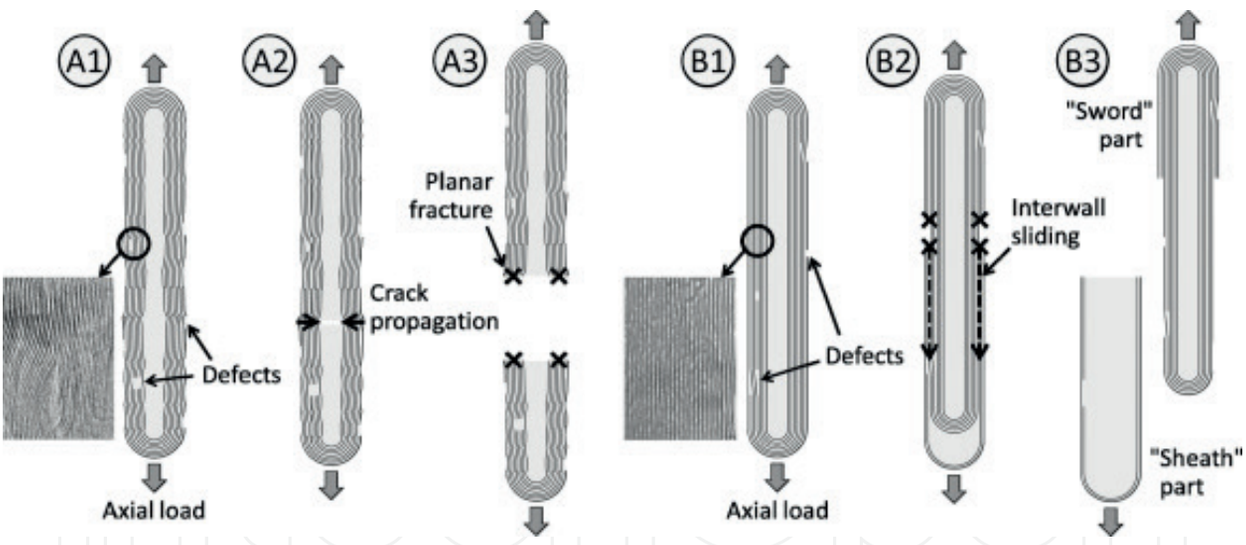

Figure 6. Schematic description of possible fracture mechanisms of MWCNTs annealed at different temperatures [53]. Shown are examples of (A1–A3) *clean break*-type failure and (B1–B3) *sword-in-sheath*-type failure.

the other fragment of the same MWCNT attached to the force-sensing cantilever had a length of approximately 3.8 μm (**Figure 7b2**). Thus, the sum of the fragment lengths (4.3 μm) exceeded the original section length. However, the length of the sword part of the nanotube (1.1 μm, **Figure 7c**) was shorter than that of the MWCNT attached to the high-force constant cantilever tip (1.9 μm). This suggests that the inner walls may break at positions that are far away from the outer walls, as shown in **Figure 7d**. This behavior can explain the *sword and sheath failure*. Of the 23 tested as-grown S-MWCNTs, 9 MWCNTs fractured as a *clean break*, and the remaining 14 MWCNTs failed leaving a *sword and sheath failure*.

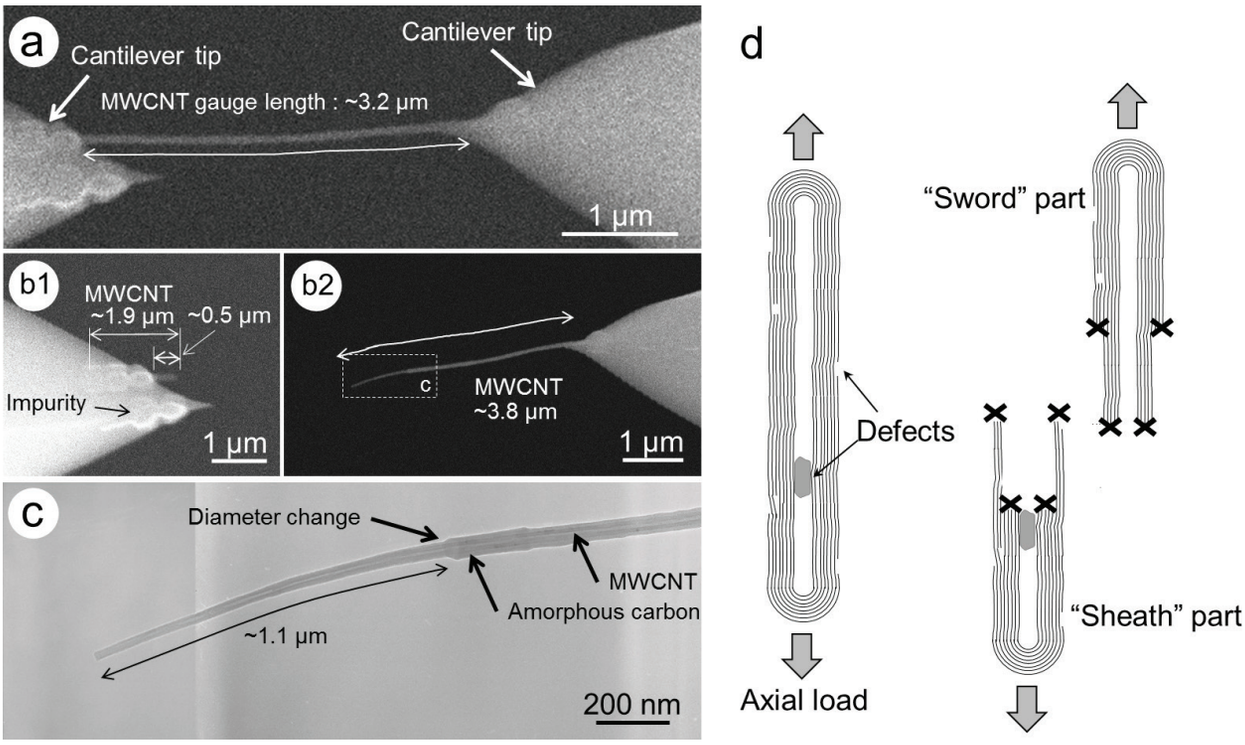

Figure 7. SEM images of S-MWCNT (a) before and (b) after the tensile test [54]. TEM image of the broken MWCNT is indicated in (c). TEM image in (c) shows the tips of the MWCNT that failed leaving the sword and sheath failure. (d) Schematic description of sword and sheath failure.

In addition to the evaluation of the fracture behavior of the MWCNTs mentioned above, we identified the fracture locations of individual S-MWCNTs broken in the uniaxial tensile tests using a piezo manipulator inside the vacuum chamber of the SEM and TEM. Of the five tested MWCNTs, three MWCNTs underwent failure at a *discontinuous flaw*, and the remaining two MWCNTs fractured at a *kink and bend*. A series of TEM images for an individual as-grown S-MWCNT, captured before and after breaking, are shown in **Figure 8**. We found that the fracture of this MWCNT occurred at a *kink and bend* structure and occurred as a *clean break*. **Figure 9** shows the characteristic features observed in a MWCNT, which fractured at a *discontinuous flaw*. The MWCNT fractured leaving a *sword and sheath failure* (**Figure 7d**). Furthermore, this MWCNT featured *hole defects* on the surface of its outer wall and the fracture occurred at a *hole defect*. This finding suggests that the fracture properties of such MWCNTs are dominated by the aforementioned structural defects.

3.2. Mechanical properties

The dependences of the nominal tensile strength upon the fracture cross section ratio and Raman intensity ratio are shown in **Figure 10**. The fracture cross section ratio was calculated by dividing the fractured cross-sectional area by the full cross-sectional area of the MWCNTs, including the inner hole. A higher fracture cross section ratio (for a given outer diameter) means a larger number of fractured walls in the MWCNT. It can

http://dx.doi.org/10.5772/intechopen.70578

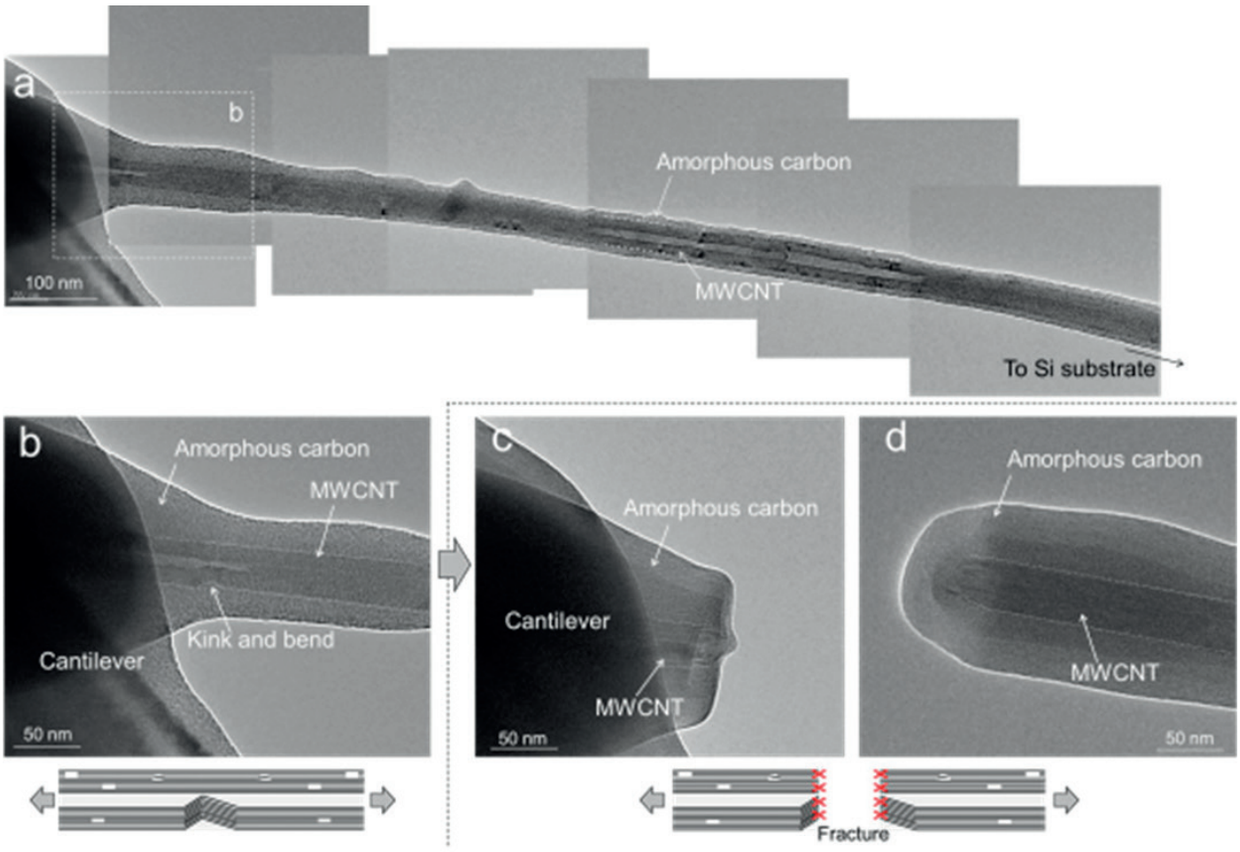

Figure 8. TEM images of S-MWCNT fractured at the *kink and bend* (a, b) before and (c, d) after the tensile test [52].

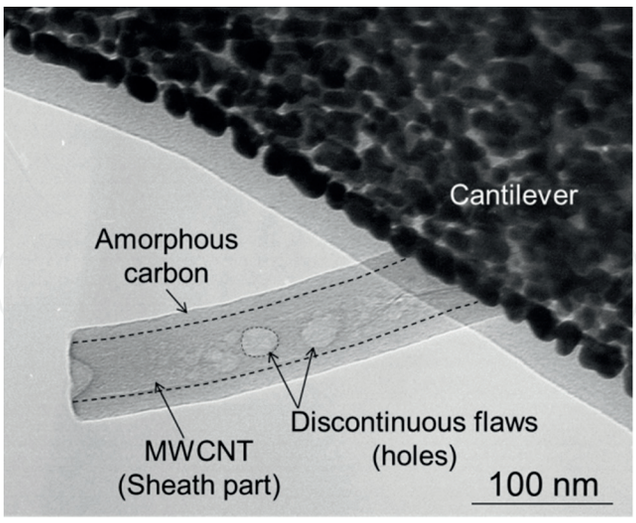

Figure 9. TEM image of S-MWCNT fractured at the *discontinuous flaw* [52].

be seen from **Figure 10a** that the H-MWCNTs annealed at 1800 and 2200°C and the as-grown S-MWCNTs had an intermediate level of crystallinity, as measured from the Raman intensity ratio (R = 1.4–4.9), compared with that of the H-MWCNTs thermally

annealed at 1200 and 2600°C (*R* values of 1.0 and 10.1, respectively). **Figure 10b** shows that the MWCNTs with an intermediate level of crystallinity produced complete fracture of the nanotube walls (*clean break* or *sword and sheath failure*) and exhibited higher nominal tensile strength. The slightly lower value of the fracture cross section ratio of the as-grown S-MWCNTs compared with that of the H-MWCNTs thermally annealed at 1800 and 2200°C was caused by the larger hollow core. Although the H-MWCNTs annealed at 1200°C failed in a *clean break* manner (**Figure 10b**), their nominal tensile strength was observed to be small (~1 GPa) because of their relatively low crystallinity (*R* = 1.0) which reflects their amorphous graphite structure and many defects. The amorphous structure might explain the low load-bearing ability of these MWCNTs. When the annealing temperature was 2600°C, an abrupt decrease in both the nominal tensile strength and the fracture cross section ratio was observed, although the crystallinity considerably increased (*R* = 10.1). This result can be attributed to a decrease in the number of cross-linking defects, i.e., interwall sp^3 bonding, owing to the high-temperature thermal annealing. The removal of cross-linking defects decreases the load transfer from the outer walls to the inner ones, resulting in multiwall-type *sword-in-sheath failure* (i.e., decrease of the fracture cross section ratio) and degradation of the load-bearing ability. These results suggest that improvements to the nominal tensile strength of MWCNTs might be achieved by inducing appropriate interactions between adjacent nanotube walls to enable sufficient load transfer to the MWCNT inner layers. This effect should be balanced to permit an adequate load transfer between the inner and outer walls to give *clean break* fractures. On the other hand, the nominal tensile strength for the thermally annealed S-MWCNTs at 2900°C shows nearly the same value as that

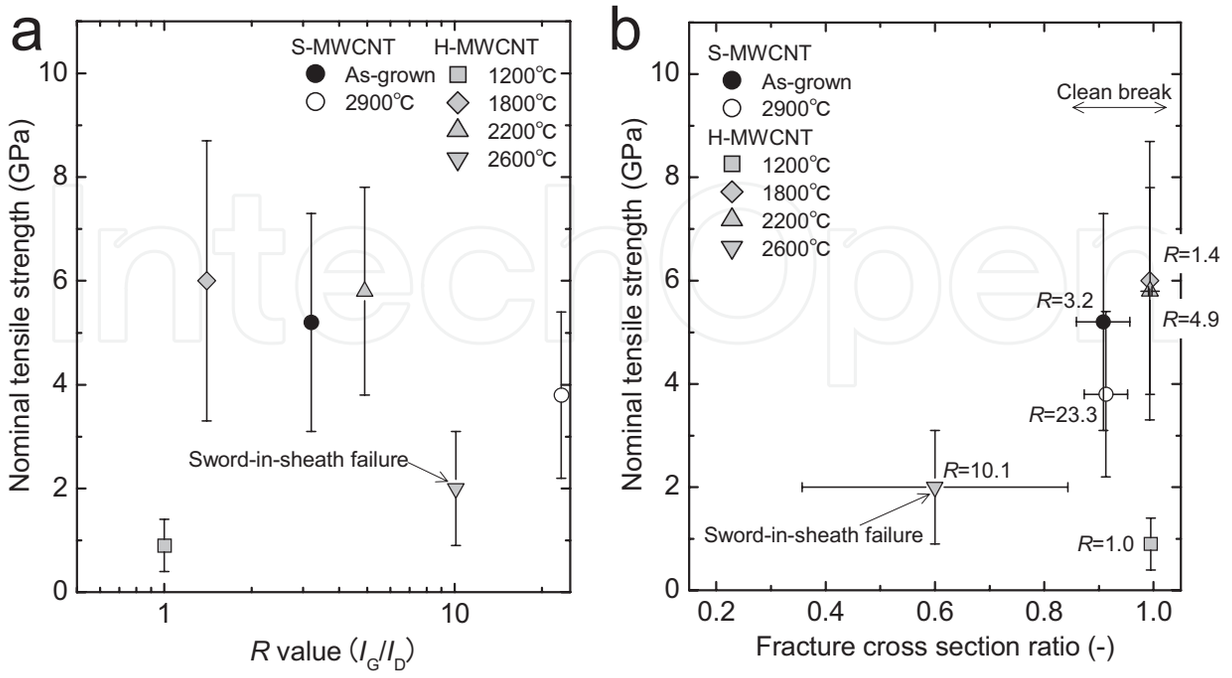

Figure 10. Nominal tensile strength of the MWCNTs as a function of (a) Raman intensity ratio and (b) fracture cross section ratio [52].

of the as-grown S-MWCNTs, even though a slight decrease in the strength is observed for the thermally annealed S-MWCNTs. This result suggests that the structural changes observed over this annealing temperature range may not have a significant impact on the nominal tensile strength of the S-MWCNTs. The H-MWCNTs had small defects, such as vacancies, Stone-Wales defects, or cross-linking defects, but no *discontinuous flaws* and *kinks and bends*, as shown in the S-MWCNTs. As a result, thermal annealing led to a decrease in the small defects with concomitant increases in the nominal tensile strength (0.9 to 5.9 GPa). On the other hand, although the as-grown S-MWCNTs exhibit an intermediate level of crystallinity (R = 3.2), they include structural defects such as *discontinuous flaws* and *kinks and bends*. Such structural defects and *hole defects* were still observed in the thermally annealed S-MWCNTs (**Table 1**). Thus, the annealing treatments led to no major changes in the controlling defects and had no major effects on the fracture morphology and nominal tensile strength of the S-MWCNTs, despite their high crystallinity.

3.3. Weibull distribution

A Weibull plot of the nominal tensile strength of the MWCNTs is shown in **Figure 11**. Supplementing the experimental results of this study, **Figure 11** also gives some results evaluated using data from the literature for previously reported CVD-grown MWCNTs and arc discharge-grown MWCNTs [37, 38, 40, 52, 53]. These nominal values were calculated based on the literature values. **Table 2** shows the outer diameter, nominal tensile strength, and Weibull scale and shape parameters of the MWCNTs. As with other brittle materials, the strength distribution of CNTs does not follow a Gaussian distribution, and failure of nanotubes is described by Weibull-Poisson statistics. If σ_{nom} is the failure strength of a nanotube, the cumulative distribution function $f(\sigma_{nom})$ for the two-parameter Weibull distribution is defined as [39]:

$$f_{(\sigma_{nom})} = 1 - \exp\left[-\left(\frac{\sigma_{nom}}{\alpha}\right)^{\beta}\right] \tag{2}$$

where $f(\sigma_{nom})$ is the probability of failure, α is the scale parameter, and β is the shape parameter. The β values of the MWCNTs are calculated to be in the range of 1.6–3.0. The comparatively low value of the shape parameter for MWCNTs indicates a wide variability in their tensile strength, more so than that of carbon fibers [60] and SiC fibers [61] (β = 15 and 7–11, respectively). This may result from the irregular nanotube structure, which reflects a larger tube defect density relative to carbon fibers and SiC fibers.

4. Conclusions

In this chapter, we reviewed the nominal tensile strength and Weibull scale and shape parameters of the nominal tensile strength distribution of MWCNTs based on our recent previous studies. The comparatively low value of the shape parameter for MWCNTs resulted

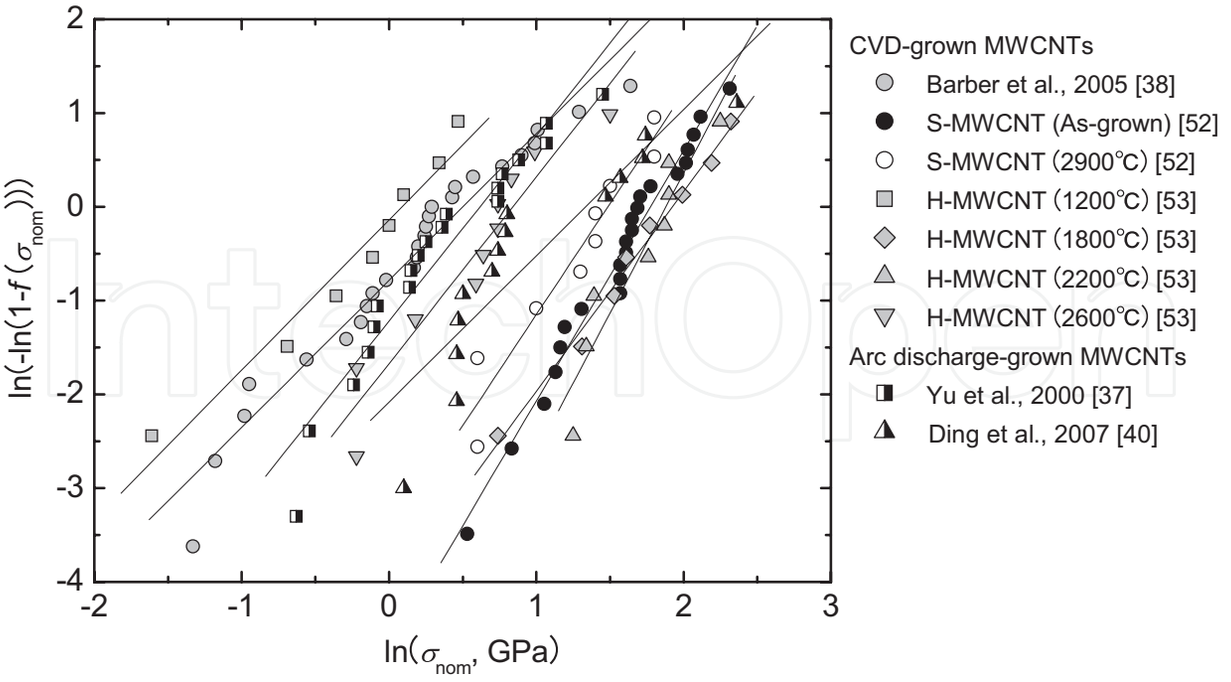

Figure 11. Weibull plot for the nominal tensile strength of MWCNTs [52].

MWCNT type	Outer diameter (nm)	Nominal tensile strength (GPa)	Scale parameter, α (GPa)	Shape parameter, β (–)	Ref.
Arc-discharge-grown	25 ± 7	1.6 ± 1.0	1.9	2.0	[37]
CVD-grown	97 ± 25	1.5 ± 1.1	1.7	1.6	[38]
Arc-discharge-grown	11 ± 3	3.4 ± 2.6	3.8	1.6	[40]
S-MWCNT (CVD, as-grown)	36 ± 7	5.2 ± 2.1	5.9	2.7	[52]
S-MWCNT (CVD, 2900°C)	35 ± 6	3.8 ± 1.6	4.4	2.4	[52]
H-MWCNT (CVD, 1200°C)	90 ± 40	0.9 ± 0.5	1.1	1.6	[53]
H-MWCNT (CVD, 1800°C)	72 ± 21	6.0 ± 2.7	6.8	2.1	[53]
H-MWCNT (CVD, 2200°C)	69 ± 16	5.8 ± 2.0	6.6	3.0	[53]
H-MWCNT (CVD, 2600°C)	67 ± 12	2.0 ± 1.1	2.3	2.0	[53]

Table 2. Measured properties for MWCNTs. Shown are the outer diameter, nominal tensile strength, and Weibull scale and shape parameters. The outer diameter and nominal tensile strength data are presented as average values ± standard deviations.

from the irregular nanotube structure, which reflects a larger tube defect density relative to conventional fiber materials. Nonetheless, the MWCNTs with an intermediate level of crystallinity produced complete fracture of nanotube walls and exhibited higher nominal

tensile strength, suggesting that there is an optimal nanotube defect density for increasing the nominal tensile strength, not too low but also not too high, so as to permit an adequate load transfer between the nanotube walls. To improve the properties of macroscopic CNT composite performance, the structure and properties of MWCNT yarns and sheets must be optimized at all hierarchical levels: from individual MWCNTs to MWCNT bundles, MWCNT networks, and MWCNT yarns and sheets. Future research efforts aimed at each of the following levels should be pursued to improve mechanical properties, particularly the nominal tensile strength of CVD-grown MWCNTs: (1) improved synthesis methods should be developed to reduce structural defects such as *discontinuous flaws* and *kinks and bends*; and (2) the degree of inter-wall cross-linking and load transfer between adjacent nanotube walls should be optimized by posttreatments, such as thermal annealing and electron irradiation. We believe that the above improvements might enable the realization of higher nominal tensile strength. More well-defined CNT architectures should contribute to enhanced mechanical properties as well as improved the electrical and thermal properties of MWCNT yarns and composites.

Acknowledgements

The authors thank Toyo Tanso Co., Ltd. for its technical assistance in thermal annealing of the MWCNTs. The authors acknowledge Prof. Y. Inoue and Prof. Y. Shimamura of Shizuoka University for their useful guidance; Dr. T. Miyazaki of the Technical Division, School of Engineering, Tohoku University, for technical assistance in the TEM analysis; Prof. K. Hirahara of Osaka University and R. Bekarevich of the National Institute for Material Science for technical assistance in the tensile testing; and our colleague, Mr. I. Tamaki of the Fracture and Reliability Research Institute (FRRI), Tohoku University, for helpful discussions. We thank Joshua Green, MS, from Edanz Group (www.edanzediting.com/ac) for editing a draft of this manuscript. This research was supported in part by the Japan Society for the Promotion of Science (JSPS) Core-to-Core Program. This research was partially supported by a Grant-in-Aid for Young Scientists (B) 16 K20904 and a Grant-in-Aid for Young Scientists (A) 15H05502.

Author details

Keiichi Shirasu[1]*, Go Yamamoto[2], Daniel Nelias[3] and Toshiyuki Hashida[1]

*Address all correspondence to: keiichi.shirasu@rift.mech.tohoku.ac.jp

1 Fracture and Reliability Research Institute, Tohoku University, Sendai, Japan

2 Department of Aerospace Engineering, Tohoku University, Sendai, Japan

3 Univ Lyon, INSA-Lyon, Villeurbanne, France

References

[1] Ruoff RS, Lorents DC. Mechanical and thermal properties of carbon nanotubes. Carbon. 1995;**33**:925-930

[2] Ebbesen TW, Lezec HJ, Hiura H, Bennett JW, Ghaemi HF, Thio T. Electrical conductivity of individual carbon nanotubes. Nature. 1996;**382**:54-56

[3] Yoshida Y. High-temperature shrinkage of single-walled carbon nanotube bundles up to 1600 K. Journal of Applied Physics. 2000;**87**:3338-3341

[4] Maniwa Y, Fujiwara R, Kira H, Tou H, Kataura H, Suzuki S, et al. Thermal expansion of single-walled carbon nanotube (SWNT) bundles: X-ray diffraction studies. Physical Review B. 2001;**64**(R):241402

[5] Schelling PK, Keblinski P. Thermal expansion of carbon structures. Physical Review B. 2003;**68**:035425

[6] Kwon YK, Berber S, Tománek D. Thermal contraction of carbon fullerenes and nanotubes. Physical Review Letters. 2004;**92**:015901

[7] Jiang H, Liu B, Huang Y, Hwang KC. Thermal expansion of single wall carbon nanotubes. Journal of Engineering Materials and Technology. 2004;**126**:265-270

[8] Hu N, Jia B, Arai M, Yan C, Li J, Liu Y, Atobe S, Fukunaga H. Prediction of thermal expansion properties of carbon nanotubes using molecular dynamics simulations. Computational Materials Science. 2012;**54**:249-254

[9] Shirasu K, Yamamoto G, Tamaki I, Ogasawara T, Shimamura Y, Inoue Y, Hashida T. Negative axial thermal expansion coefficient of carbon nanotubes: Experimental determination based on measurements of coefficient of thermal expansion for aligned carbon nanotube reinforced epoxy composites. Carbon. 2015;**95**:904-909

[10] Shirasu K, Nakamura A, Yamamoto G, Ogasawara T, Shimamura Y, Inoue Y, Hashida T. Potential use of CNTs for production of zero thermal expansion coefficient composite materials: An experimental evaluation of axial thermal expansion coefficient of CNTs using a combination of thermal expansion and uniaxial tensile tests. Composites Part A: Applied Science and Manufacturing. 2017;**95**:152-160

[11] Peng B, Locascio M, Zapol P, Li S, Mielke SL, Schatz GC, Espinosa HD. Measurements of near-ultimate strength for multiwalled carbon nanotubes and irradiation-induced cross-linking improvements. Nature Nanotechnology. 2008;**3**:626-631

[12] Locascio M, Peng B, Zapol P, Zhu Y, Li S, Belytschko T, Espinosa HD. Tailoring the load carrying capacity of MWCNTs through inter-shell atomic bridging. Experimental Mechanics. 2009;**49**:169-182

[13] Zhang M, Atkinson KR, Baughman RH. Multifunctional carbon nanotube yarns by downsizing an ancient technology. Science. 2004;**306**:1358-1361

[14] Zhang M, Fang S, Zakhidov AA, Lee SB, Aliev AE, Williams CD. Strong, transparent, multifunctional, carbon nanotube sheets. Science. 2005;**309**:1215-1219

[15] Cheng Q, Wang J, Jiang K, Li Q, Fan S. Fabrication and properties of aligned multi-walled carbon nanotube-reinforced epoxy composites. Journal of Materials Research. 2008;**23**:2975-2983

[16] Cheng Q, Bao J, Park JG, Liang Z, Zhang C, Wang B. High mechanical performance composite conductor: Multi-walled carbon nanotube sheet/bismaleimide nanocomposites. Advanced Functional Materials. 2009;**19**:3219-3225

[17] Cheng QF, Wang JP, Wen JJ, Liu CH, Jiang KL, Li QQ, Fan SS. Carbon nanotube/epoxy composites fabricated by resin transfer molding. Carbon. 2010;**48**:260-266

[18] Bradford PD, Wang X, Zhao H, Maria JP, Jia Q, Zhu YT. A novel approach to fabricate high volume fraction nanocomposites with long aligned carbon nanotubes. Composites Science and Technology. 2010;**70**:1980-1985

[19] Cheng Q, Wang B, Zhang C, Liang Z. Functionalized carbon-nanotube sheet/bismaleimide nanocomposites: Mechanical and electrical performance beyond carbon-fiber composites. Small. 2010;**6**:763-767

[20] Ogasawara T, Moon SY, Inoue Y, Shimamura Y. Mechanical properties of aligned multi-walled carbon nanotube/epoxy composites processed using a hot-melt prepreg method. Composites Science and Technology. 2011;**71**:1826-1833

[21] Liu W, Zhang X, Xu G, Bradford PD, Wang X, Zhao H, Zhang Y, Jia Q, Yuan FG, Li Q, Qiu Y, Zhu Y. Producing superior composites by winding carbon nanotubes onto a mandrel under a poly(vinyl alcohol) spray. Carbon. 2011;**49**:4786-4791

[22] Wang X, Bradford PD, Liu W, Zhao H, Inoue Y, Maria JP, Li Q, Yuan FG, Zhu Y. Mechanical and electrical property improvement in CNT/nylon composites through drawing and stretching. Composites Science and Technology. 2011;**71**:1677-1683

[23] Liu W, Zhao H, Inoue Y, Wang X, Bradford PD, Kim H, Qui Y, Zhu Y. Poly(vinyl alcohol) reinforced with large-diameter carbon nanotubes via spray winding. Composites Part A: Applied Science and Manufacturing. 2012;**43**:587-592

[24] Wang X, Yong ZZ, Li QW, Bradford PD, Liu W, Tucker DS, Cai W, Yuan FG, Zhu YT. Ultrastrong, stiff and multifunctional carbon nanotube composites. Materials Research Letters. 2013;**1**:19-25

[25] Mikhalchan A, Gspann T, Windle A. Aligned carbon nanotube-epoxy composites: The effect of nanotube organization on strength, stiffness, and toughness. Journal of Materials Science. 2016;**51**:10005-10025

[26] Di J, Wang X, Xing Y, Zhang Y, Zhang X, Lu W, Li Q, Zhu YT. Dry-processable carbon nanotubes for functional devices and composites. Small. 2014;**10**:4606-4625

[27] Goh PS, Ismail AF, Ng BC. Directional alignment of carbon nanotubes in polymer matrices: Contemporary approaches and future advances. Composites Part A: Applied Science and Manufacturing. 2014;**56**:103-126

[28] Salvetat JP, Kulik AJ, Bonard JM, Briggs GAD, Stöckli T, Méténier K, Bonnamy S, Béguin F, Burnham NA, Forró L. Elastic modulus of ordered and disordered multiwalled carbon nanotubes. Advanced Materials. 1999;**11**:161-165

[29] Yamamoto G, Suk JW, An J, Piner RD, Hashida T, Takagi T, Ruoff RD. The influence of nanoscale defects on the fracture of multi-walled carbon nanotubes under tensile loading. Diamond and Related Materials. 2010;**19**:748-751

[30] Elumeeva KV, Kuznetsov VL, Ischenko AV, Smajda R, Spina M, Forró L, Magrez A. Reinforcement of CVD grown multi-walled carbon nanotubes by high temperature annealing. AIP Advances. 2013;**3**:112101

[31] Kimura T, Suzuki H, Zhang M, Yamamoto G, Hashida T, Motomiya K, Tohji K, Sato Y. Is the tensile strength of carbon nanotubes enhanced by supported materials?: Effect of supported amorphous alumina nanoparticles on the tensile strength of carbon nanotubes. Carbon. 2017;**118**:339-342

[32] Ogata S, Shibutani Y. Ideal tensile strength and band gap of single-walled carbon nanotubes. Physical Review B. 2003;**68**:165409

[33] Ozaki T, Iwasa Y, Mitani T. Stiffness of single-walled carbon nanotubes under large strain. Physical Review Letters. 2000;**84**:1712-1715

[34] Dumitrică T, Belytscko T, Yakobson BI. Bond-breaking bifurcation states in carbon nanotube fracture. Journal of Chemical Physics. 2003;**118**:9485-9488

[35] Mielke SL, Troya D, Zhang S, Li JL, Xiao S, Car R, Ruoff RS, Schatz GC, Belytschko T. The role of vacancy defects and holes in the fracture of carbon nanotubes. Chemical Physics Letters. 2004;**390**:413-420

[36] Troya D, Mielke SL, Schatz GC. Carbon nanotube fracture-differences between quantum mechanical mechanisms and those of empirical potentials. Chemical Physics Letters. 2003;**382**:133-141

[37] Yu MF, Lourie O, Dyer MJ, Moloni K, Kelly TF, Ruoff RS. Strength and breaking mechanism of multiwalled carbon nanotubes under tensile load. Science. 2000;**287**:637-640

[38] Barber AH, Andrews R, Schadler LS, Wagner HD. On the tensile strength distribution of multiwalled carbon nanotubes. Applied Physics Letters. 2005;**87**:213106

[39] Barber AH, Kaplan-Ashiri I, Cohen SR, Tenne R, Wagner HD. Stochastic strength of nanotubes: An appraisal of available data. Composites Science and Technology. 2005;**65**:2380-2384

[40] Ding W, Calabri L, Kohlhaas KM, Chen X, Dikin DA, Ruoff RS. Modulus, fracture strength, and brittle vs. plastic response of the outer shell of arc-grown multi-walled carbon nanotubes. Experimental Mechanics. 2007;**47**:25-36

[41] Zhang B, Zhao L, Cheng Y, Golberg D, Wang MS. Reversible tuning of individual carbon nanotube mechanical properties via defect engineering. Nano Letters. 2016;**16**:5221-5227

[42] Tombler TW, Zhou C, Alexseyev L, Kong J, Dai H, Liu L, Jayanthi CS, Tang M, SY W. Reversible electromechanical characteristics of carbon nanotubes under local-probe manipulation. Nature. 2000;**405**:769-772

[43] Lukić B, Seo JW, Bacsa RR, Delpeux S, Béguin F, Bister G, Fonseca A, Nagy JB, Kis A, Jeney S, Kulik AJ, Forró L. Catalytically grown carbon nanotubes of small diameter have a high Young's modulus. Nano letters. 2005;**5**:2074-2077

[44] Lukić B, Seo JW, Couteau E, Lee K, Gradečak S, Berkecz R, Hernadi K, Delpeux S, Cacciaguerra T, Béguin F, Fonseca A, Nagy JB, Csányi G, Kis A, Kulik AJ, Forró L. Elastic modulus of multi-walled carbon nanotubes produced by catalytic chemical vapour deposition. Applied Physics A. 2005;**80**:695-700

[45] Lee K, Lukić B, Magrez A, Seo JW, Andrew G, Briggs D, Kulik AJ, Forró L. Diameter-dependent elastic modulus supports the metastable-catalyst growth of carbon nanotubes. Nano Letters. 2007;**7**:1598-1602

[46] Duchamp M, Meunier R, Smajda R, Mionic M, Magrez A, Seo JW, Forró L, Song B, Tománek D. Reinforcing multiwall carbon nanotubes by electron beam irradiation. Journal of Applied Physics. 2010;**108**:084314

[47] Poncharal P, Wang ZL, Ugarte D, de Heer WA: Electrostatic deflections and electromechanical resonances of carbon nanotubes. Science. 1999;**283**:1513-1516

[48] Gaillard J, Skove M, Rao AM. Mechanical properties of chemical vapor deposition-grown multiwalled carbon nanotubes. Applied Physics Letters. 2005;**86**:233109

[49] Yu MF, Files BS, Arepalli S, Ruoff RS. Tensile loading of ropes of single wall carbon nanotubes and their mechanical properties. Physical Review Letters. 2000;**84**:5552-5555

[50] Demczyk BG, Wang YM, Cumings J, Hetman M, Han W, Zettl A, Ritchie RO. Direct mechanical measurements of the tensile strength and elastic modulus of multi-walled carbon nanotubes. Material Science and Engineering A. 2002;**A334**:173-178

[51] Wang MS, Golberg D, Bando Y. Tensile tests on individual single-walled carbon nanotubes: Linking nanotube strength with its defects. Advanced Materials. 2010;**22**: 4071-4075

[52] Shirasu K, Tamaki I, Miyazaki T, Yamamoto G, Bekarevich R, Hirahara K, Shimamura Y, Inoue Y, Hashida T. Key factors limiting carbon nanotube strength: Structural characterization and mechanical properties of multi-walled carbon nanotubes. Mechanical Engineering Journal. 2017;**4**:17-00029. DOI: 10.1299/mej.17-00029

[53] Yamamoto G, Shirasu K, Nozaka Y, Sato Y, Takagi T, Hashida T. Structure-property relationships in thermally-annealed multi-walled carbon nanotubes. Carbon. 2014;**66**:219-226

[54] Tamaki I, Shirasu K, Miyazaki T, Yamamoto G, Bekarevich R, Hirahara K, Shimamura Y, Inoue Y, Hashida T. Effects of structural defects on strength and fracture properties of multi-walled carbon nanotubes. Transactions of the JSME (in Japanese). 2017;**83**:16-00283. DOI: 10.1299/transjsme.16-00283

[55] Inoue Y, Kakihata K, Hirono Y, Horie T, Ishida A, Mimura H. One-step grown aligned bulk carbon nanotubes by chloride mediated chemical vapor deposition. Applied Physics Letters. 2008;**92**:213113

[56] Dresselhaus MS, Dresselhaus G, Saito R, Jorio A. Raman spectroscopy of carbon nanotubes. Physics Reports. 2005;**409**:47-99

[57] Kataura H, Kumazawa Y, Maniwa Y, Ohtsuka Y, Sen R, Suzuki S, Achiba Y. Diameter control of single-walled carbon nanotubes. Carbon. 2000;**38**:1691-1697

[58] Sader JE, Chon JWM, Mulvaney P. Calibration of rectangular atomic force microscope cantilevers. Review of Scientific Instruments. 1999;**70**:3967-3969

[59] Ding W, Dikin DA, Chen X, Piner RD, Ruoff RS, Zussman E, Wang X, Li X. Mechanics of hydrogenated amorphous carbon deposits from electron-beam-induced deposition of a paraffin precursor. Journal of Applied Physics. 2005;**98**:014905

[60] Okabe T, Takeda N. Elastoplastic shear-lag analysis of single-fiber composites and strength prediction of unidirectional multi-fiber composites. Composites Part A: Applied Science and Manufacturing. 2002;**33**:1327-1335

[61] Curtin WA, Netravali AN, Park JM. Strength distribution of Carborundum polycrystalline SiC fibres as derived from the single-fibre-composite test. Journal of Materials Science. 1994;**29**:4718-4728